

Article

Tensile Stress Evolution Outside Deformation Zone of Cold Rolled Strip

Kangwu Zhang^{1,2}, Dongcheng Wang^{1,2,3,*}, Yanghuan Xu¹ and Hongmin Liu^{1,3}

¹ National Engineering Research Center for Equipment and Technology of Cold Rolling Strip, Yanshan University, Qinhuangdao 066004, China; yhsj220436@163.com (K.Z.); xyh@stumail.ysu.edu.cn (Y.X.); liuhmin@ysu.edu.cn (H.L.)

² National Key Laboratory of Metal Forming Technology and Heavy Equipment, China National Heavy Machinery Research Institute Co., Ltd., Xi'an 710032, China

³ State Key Laboratory of Metastable Materials Science and Technology, Yanshan University, Qinhuangdao 066004, China

* Correspondence: wangdongcheng@ysu.edu.cn

Abstract: To determine the exact distribution of tensile stress in a cold rolled strip, tensile stress evolution caused by lateral uneven velocity distribution outside the deformation zone of the strip is examined. The finite difference method is employed to solve the problem. Different factors, including the strip width and the form and amplitude of the initial stress distribution on the stress evolution, are analyzed. On the one hand, to improve the calculation speed, a “Gaussian” curve is proposed to fit the results calculated by the finite difference method. Simulation results show that the stress evolution calculated by the fitting equation is in good agreement with that obtained by the finite difference method. On the other hand, to verify the exactness of the model, an experiment is conducted, and the comparison between the calculated results and experimental values is discussed.

Keywords: cold rolling; tensile stress; velocity distribution; finite difference method; experiment



Citation: Zhang, K.; Wang, D.; Xu, Y.; Liu, H. Tensile Stress Evolution Outside Deformation Zone of Cold Rolled Strip. *Appl. Sci.* **2023**, *13*, 6781. <https://doi.org/10.3390/app13116781>

Academic Editors: Michael Oluwatosin Bodunrin, Desmond Klenam and Japheth Obiko

Received: 11 May 2023

Revised: 29 May 2023

Accepted: 30 May 2023

Published: 2 June 2023



Copyright: © 2023 by the authors. Licensee MDPI, Basel, Switzerland. This article is an open access article distributed under the terms and conditions of the Creative Commons Attribution (CC BY) license (<https://creativecommons.org/licenses/by/4.0/>).

1. Introduction

Cold rolled strips are widely used in automobiles, households, buildings, and the electronics industry [1–3]. The accuracy of its flatness and thickness is important in a cold rolled strip. With the rapid development of science and technology, such thin strips are playing an increasingly important role in industry. At the same time, demand for cold rolled strips with high-quality flatness is increasing [4–6].

The stress distribution in a cold rolled strip has a significant impact on its flatness quality. Thus, establishing a model of the stress distribution is of considerable interest to many researchers. The earliest stress distribution model for cold rolled strips was presented by Shohet and Townsend [7], which is widely used by many researchers [8,9]. To determine the precise stress distribution, researchers proposed various methods, such as the analytical method [10–12], three-dimensional difference method [13], finite element method [14], variation method [15,16], and strip element method [17,18]. Although the aforementioned models gained widespread support from industrialists and academics, they suffer from certain major drawbacks. As shown in Figure 1 [19,20], the analytical method is based on the assumption that the stress distribution far upstream (point A) has no effect on the stress distribution at the roll-gap entry (point B), exit (point C), and far downstream (point D), and at the same time, the stress distribution at points B, C, and D is identical. In contrast, the three-dimensional difference method does not consider the influence of residual stress at point A and analyzes the transverse distribution of residual stress at points B and C. It does not indicate whether the tensile stresses at points C and D are the same. Meanwhile, the variation method and strip element method are based on the hypothesis that the stress distribution at points C and D is identical. While the former method considers the stress

distribution at points A and B to be identical, the latter method considers the uneven velocity distribution at point B, so the stress distribution at point B is the sum of the stress distribution at point A and the additional stress distribution caused by the uneven velocity distribution at point B.

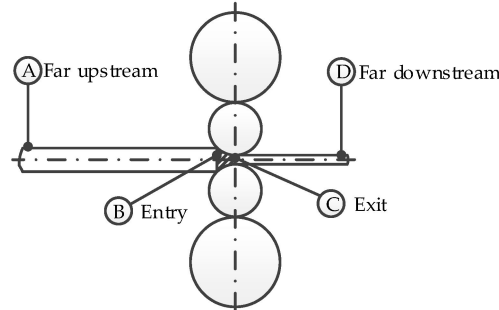


Figure 1. Typical location of strip in cold rolling.

The stress distribution at points A, B, C, and D is different [21–23]. As the velocity distribution at points B and C is uneven, the additional stress distribution caused by this uneven velocity distribution must be considered. Generally, a cold rolling shape meter can measure the uneven stress distribution; however, if the shape meter is not installed far enough from point C, then the measurements will include the residual stress and additional stress distribution caused by the uneven velocity distribution, which will have an adverse effect on the flatness control.

According to rolling theory [24], uneven tensile stress distribution will result in the uneven distribution of the rolling force, neutral point, forward slip, and backward slip along the strip width. Moreover, the uneven tensile stress distribution will eventually cause uneven velocity distribution at the entry and exit. At the same time, the uneven velocity distribution will result in uneven tensile stress distribution.

Tensile stress consists of mean tensile stress, residual stress, and the additional stress caused by the uneven velocity distribution. The tensile stress distribution is flowing, along with the change in the velocity distribution before the entry and after the exit of the deformation zone. Generally, the tensile stress, residual stress, and velocity distribution at the entry and exit of the deformation zone are coupled with one another (as shown in Figure 2). Outside the deformation zone, the velocity and tensile stress distribution is flowing (as shown in Figure 3).

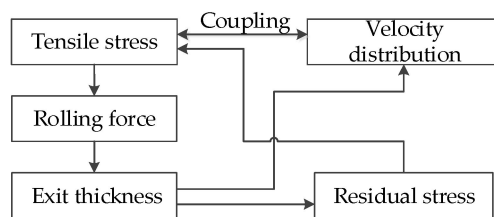


Figure 2. Coupling relationship between velocity and stress.

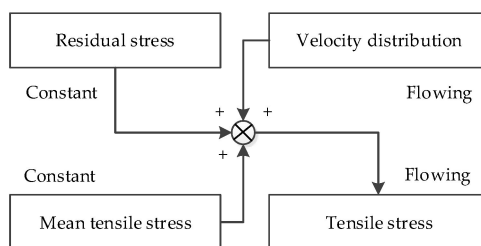


Figure 3. Combination relationship outside the deformation zone.

In a word, to determine the precise stress distribution, two problems must be solved. The first problem is the coupling at the entry and exit of the deformation zone, and the second problem is the flowing of the velocity and tensile stress distribution outside the deformation zone. This study delves into the second problem. The key to the second problem is to examine the evolution of the stress distribution between points C and D, which is similar to the evolution of the stress distribution between points A and B. However, research on this problem is limited. The only study on the subject was conducted by [25], who used a Laplace transform technique to solve the problem. With the assumption that the velocity distribution is a sine or cosine function, numerous beneficial conclusions can be obtained. Laplace transform methods are limited to some inherent characteristics, so complex velocity distributions cannot be settled easily. This work introduces the finite difference method to solve the problem. The finite difference method is suitable for complex boundary conditions. The different influencing factors, including the strip width and the form and amplitude of the initial stress caused by the uneven velocity distribution on the evolution of the stress distribution between points C and D, are analyzed in this study. Based on the simulation results, a new formula is obtained, which can be used to calculate the evolution of the stress distribution easily and quickly, with high precision.

To verify the exactness of the model, an experiment is conducted, and the comparison between the calculated results and experimental values is discussed.

2. Governing Equations

2.1. Problem Description

The strip is assumed to be very thin, making the problem a two-dimensional plane stress problem. As shown in Figure 4, x is the width direction, y is the rolling direction, and B is the strip width. From the exit of the deformation zone, the area of $B \times 2B$ is analyzed. According to [25], $2B$ is an adequate distance for the velocity distribution, evolving from uneven to even, so at $y = 2B$, the stress $\sigma_y(x)$ induced by the velocity distribution is 0. At $x = -B/2$ and $x = B/2$, the surface force of F_x and F_y is 0, and at $y = 0$, the stress $\sigma_y(x)$ induced by the uneven velocity distribution is expressed by Equation (1):

$$\sigma_y(x) = E \frac{\bar{v}_y - v_y}{\bar{v}_y} \tag{1}$$

where E is the Young’s modulus of the strip, v_y is the velocity distribution at the exit of the deformation zone, and \bar{v}_y is the average velocity at the exit of the deformation zone.

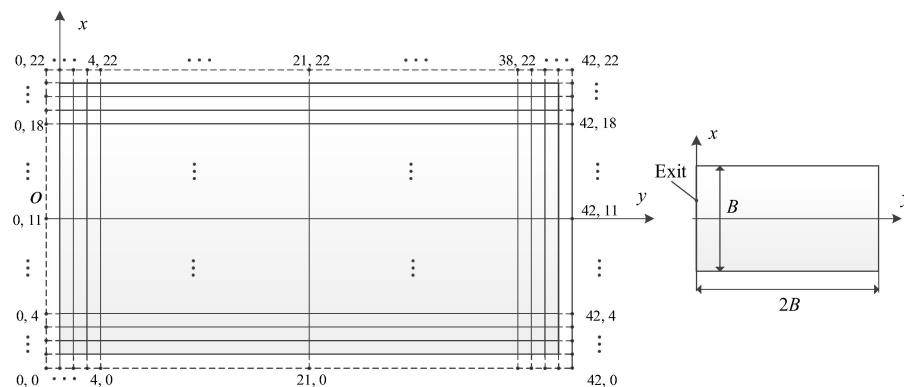


Figure 4. Coordinate system of the problem.

According to the theory of elasticity [26], the stress function of the plane stress problem can be described as the biharmonic Equation (2):

$$\frac{\partial^4 \varphi}{\partial x^4} + 2 \frac{\partial^4 \varphi}{\partial x^2 \partial y^2} + \frac{\partial^4 \varphi}{\partial y^4} = 0 \tag{2}$$

where φ is the stress function.

The boundary conditions can be described by Equation (3):

$$\begin{cases} l \frac{\partial^2 \varphi}{\partial y^2} - m \frac{\partial^2 \varphi}{\partial x \partial y} = F_x \\ m \frac{\partial^2 \varphi}{\partial x^2} - l \frac{\partial^2 \varphi}{\partial x \partial y} = F_y \end{cases} \tag{3}$$

where l, m are the directional cosines, and F_x, F_y are the applied surface force on the boundary.

To solve the problem with the finite difference method, the strip is divided into 20×40 small rectangular elements, and the side length of a small rectangular element is $B/20$. Outside the border of the strip, a layer of imaginary nodes is applied. The nodes are numbered $i = 0 \sim 42, j = 0 \sim 22$.

2.2. Solution Technique

According to the locations of the different nodes, different equations are obtained. For the inner nodes, Equation (2) can be converted into a finite difference, yielding Equation (4):

$$20\varphi_{i,j} - 8(\varphi_{i+1,j} + \varphi_{i-1,j} + \varphi_{i,j+1} + \varphi_{i,j-1}) + 2(\varphi_{i+1,j+1} + \varphi_{i-1,j+1} + \varphi_{i+1,j-1} + \varphi_{i-1,j-1}) + (\varphi_{i+2,j} + \varphi_{i-2,j} + \varphi_{i,j+2} + \varphi_{i,j-2}) = 0 \tag{4}$$

where $\varphi_{i,j}$ is stress function of node (i, j) .

For the boundary nodes, a basis point must be chosen. For convenience, node $(41, 11)$ is chosen as the basis point. The stress function and first-order partial derivative of the stress function should be equal to 0, as follows in Equation (5):

$$\varphi_{41,11} = \left(\frac{\partial \varphi}{\partial x} \right)_{41,11} = \left(\frac{\partial \varphi}{\partial y} \right)_{41,11} = 0 \tag{5}$$

According to the basic theory, the stress functions and first-order partial derivatives of the stress functions of the other boundary nodes can be calculated by Equation (6):

$$\begin{cases} \left(\frac{\partial \varphi}{\partial x} \right)_A = - \int_O^A F_y ds \\ \left(\frac{\partial \varphi}{\partial y} \right)_A = \int_O^A F_x ds \\ \varphi_A = \int_O^A (y_A - y) F_x ds + \int_O^A (x - x_A) F_y ds \end{cases} \tag{6}$$

where O is the basis point, and A is any boundary node that must be solved.

The stress functions of all the boundary nodes can be obtained according to Equation (6). In addition, from the first-order partial derivatives of the stress functions, the following equation can be obtained:

$$\begin{cases} \frac{\varphi_{2,j} - \varphi_{0,j}}{B/10} = \left(\frac{\partial \varphi}{\partial y} \right)_{1,j} (j = 1 - 21) \\ \frac{\varphi_{42,j} - \varphi_{40,j}}{B/10} = \left(\frac{\partial \varphi}{\partial y} \right)_{41,j} (j = 1 - 21) \\ \frac{\varphi_{i,2} - \varphi_{i,0}}{B/10} = \left(\frac{\partial \varphi}{\partial x} \right)_{i,1} (i = 1 - 41) \\ \frac{\varphi_{i,22} - \varphi_{i,20}}{B/10} = \left(\frac{\partial \varphi}{\partial x} \right)_{i,21} (i = 1 - 41) \end{cases} \tag{7}$$

The stress functions of the four corner nodes are meaningless to the problem. Based on Equations (4), (5) and (7), the stress function of each node can be solved. The linear systems of Equations (4), (5) and (7) are solved using the scientific computation package Scipy through the Python language.

3. Results Analysis

With the finite difference method, different influencing factors, including the strip width and the form and amplitude of the initial stress on the evolution of the stress distribution, are analyzed. To match the common stress distribution form in practice, the initial stress induced by the velocity distribution at the exit of the deformation zone is assumed to be a quartic polynomial, which can be expressed as Equation (8).

$$\sigma_y(x) = a_0 + a_2 \left(\frac{x}{B/2}\right)^2 + a_4 \left(\frac{x}{B/2}\right)^4 \tag{8}$$

where a_0 , a_2 , and a_4 are the coefficients of the quartic polynomial.

First, when the strip width is 1000 mm, the effects of different initial stress forms on the stress evolution are shown in Figures 5–8. It can be seen that the stress tends to be zero after roughly one strip width among the four types of initial stress at the exit of the deformation zone, and the variation trends of the stress evolution of the different initial forms are different. In the case of $a_2 = -100$ MPa, $a_4 = 0$ along direction y , the stress along the edge of the strip tends to be steady, while the stress in the middle of the strip presents an “S”-shaped form. A similar law can be observed in the case of $a_2 = 0$, $a_4 = 100$ MPa. In the case of $a_2 = -100$ MPa, $a_4 = 100$ MPa, the stress in the middle of the strip presents an “S”-shaped form, but the change trend of the evolution of the stress along the edge of the strip is highly complex. That is, it decreases with distance, and then it increases to zero instead of decreasing to zero directly. The case of $a_2 = 100$ MPa, $a_4 = -100$ MPa is similar to the case of $a_2 = -100$ MPa, $a_4 = 100$ MPa. According to the theory of elasticity, the superposition principle can be used. That is, the case of $a_2 = -100$ MPa, $a_4 = 100$ MPa can be treated as the superposition of $a_2 = -100$ MPa, $a_4 = 0$ and $a_2 = 0$, $a_4 = 100$ MPa. Thus, the case of $a_2 = -100$ MPa, $a_4 = 0$ and $a_2 = 0$, $a_4 = 100$ MPa can be considered as two basic modes, and any stress form combination at the exit of the deformation zone can be handled easily if the stress evolution regulation of the basic modes is known.

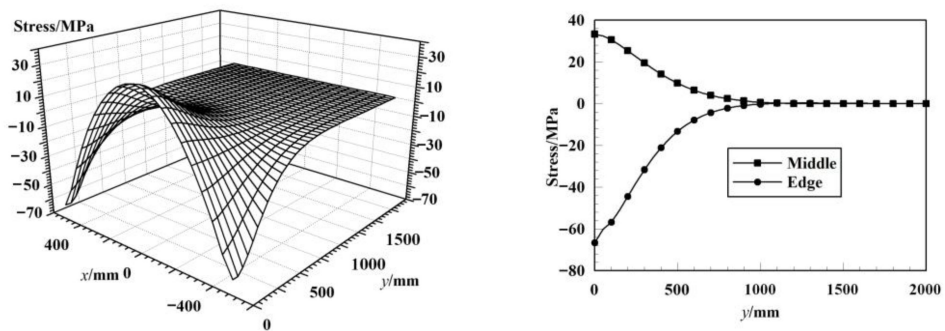


Figure 5. Results of $a_2 = -100$ MPa, $a_4 = 0$.

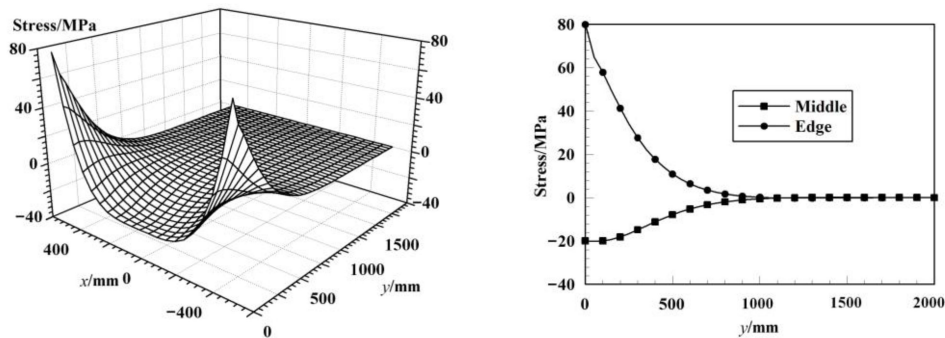


Figure 6. Results of $a_2 = 0$, $a_4 = 100$ MPa.

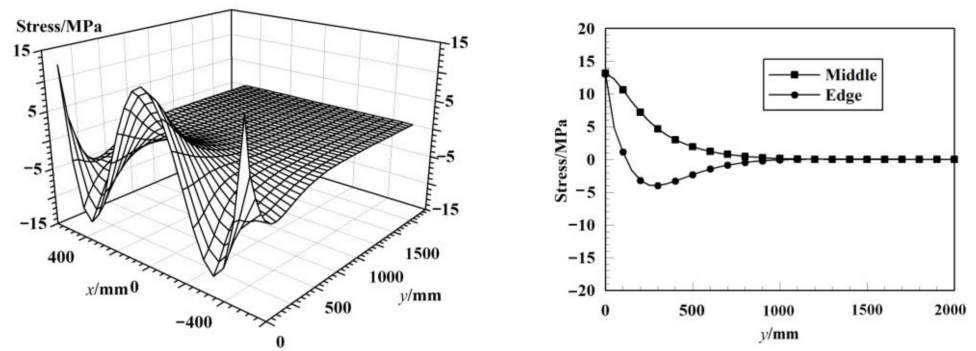


Figure 7. Results of $a_2 = -100$ MPa, $a_4 = 100$ MPa.

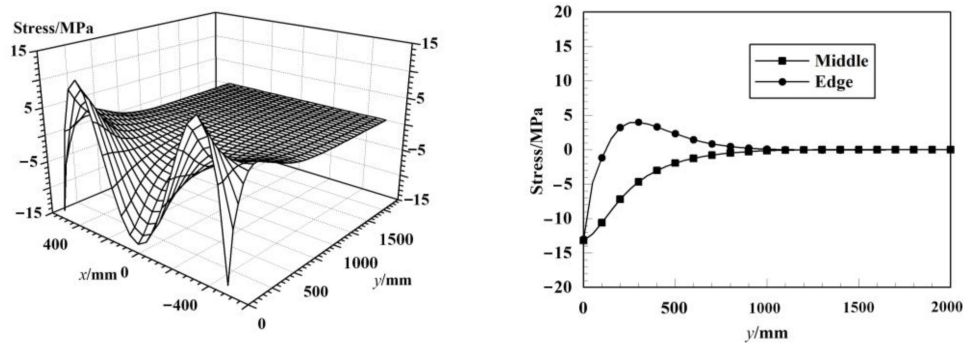


Figure 8. Results of $a_2 = 100$ MPa, $a_4 = -100$ MPa.

Second, when the strip width is 1000 mm, and $a_4 = 0$, the initial stress amplitude a_2 will be 20, 40, 60, 80, or 100 MPa. The effect of the different initial stress amplitudes on the stress evolution is shown in Figure 9. It can be seen that the form of the stress distribution is similar to the different initial stress amplitudes on the same y coordinate, and the stress amplitude on the same y coordinate has a linear relationship with the amplitude of the initial stress. In addition, it can be seen that the stress amplitudes fall roughly 98.8% compared with the original stress on $y = B$, whereas the stress on $y = B/2$ is decaying.

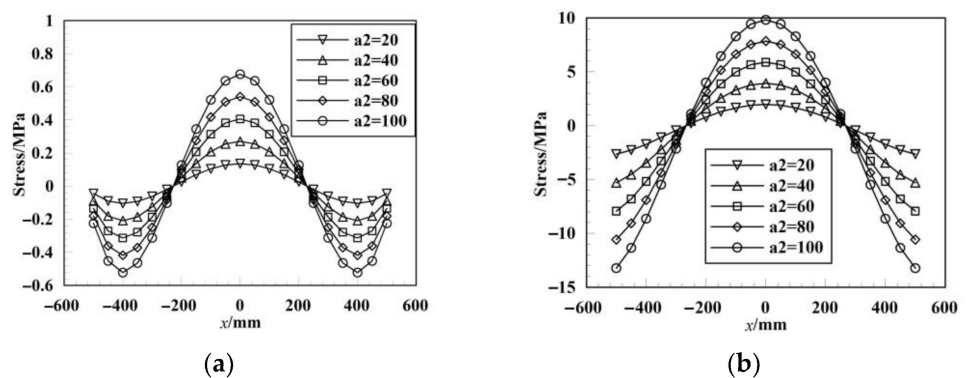


Figure 9. Results of different initial stress amplitudes. (a) $y = B$, (b) $y = B/2$.

Finally, when $a_2 = -100$ MPa, $a_4 = 0$, the strip width will be 1000, 1500, 2000, or 2500 mm, and the effect of the different strip widths on the stress evolution is shown in Figure 10. It can be seen that the different strip widths have a similar stress evolution regulation in the middle and along the edge of the strip. If the horizontal axis is y/B , then all the curves will coincide with one another.

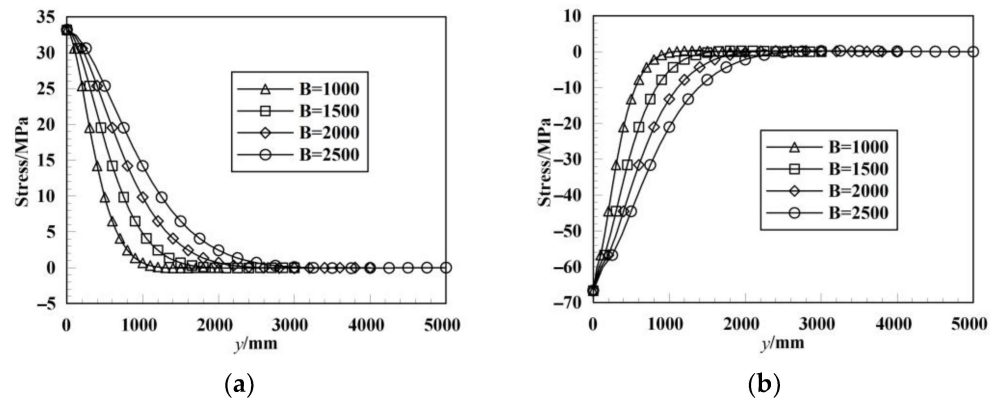


Figure 10. Results of different strip widths. (a) Stress distribution in the middle of the strip. (b) Stress distribution along the edge of the strip.

From the above analysis, it can be determined that the initial stress amplitude and strip width have little effect on the change trend of the stress evolution, and the highly influential factor is the form of the initial stress, which can be broken down into two basic modes, namely, a unit quadratic or quartic coefficient. For example, the case of $a_2 = -100$ MPa, $a_4 = 100$ MPa can be treated as the superposition of $a_2 = -100$ MPa, $a_4 = 0$ and $a_2 = 0$, $a_4 = 100$ MPa.

4. Discussion

Although the finite difference method is effective in solving the problem, its calculation speed is slow, as the calculation slows down when solving a large system of linear equations. If the calculation results of the finite difference method can be fitted by a simple equation, it will increase the computation speed significantly. A natural idea is fitting the surfaces in Figures 5 and 6 directly. However, different types of surface equations are necessary to fit the surfaces in Figures 5 and 6, and the fitting results will be unsatisfactory. Another idea is fitting the curves in Figures 5 and 6, which was also proven to be unsatisfactory. After careful consideration, it was decided that the quadratic and quartic coefficients of the different y values can be fitted by a type of “Gaussian” curve with high precision. The basic curve equation can be expressed as Equation (9).

$$f(y/B) = A_1 \exp\left(-\left(\frac{y/B - B_1}{C_1}\right)^2\right) + A_2 \exp\left(-\left(\frac{y/B - B_2}{C_2}\right)^2\right) \quad (9)$$

where $A_1, B_1, C_1, A_2, B_2,$ and C_2 are the fitting coefficients.

The fitting coefficients in Equation (9) are obtained using the numerical computation package Numpy through the Python language. The fitting results are shown in Figures 11 and 12, and Table 1. It can be seen that the fitting results of all the cases are highly satisfactory. In Figure 11, a_{20} is the quadratic coefficient of the initial stress distribution, and the quartic coefficient is zero. In Figure 12, a_{40} is the quartic coefficient of the initial stress distribution, and the quadratic coefficient is zero.

Table 1. Results of fitting coefficients.

	Mode	A_1	B_1	C_1	A_2	B_2	C_2
1	a_2	0.01292	0.03105	0.02057	1.114	-0.1145	0.6015
	a_4	-0.07125	0.3252	0.2516	-0.119	0.431	0.4751
2	a_2	0.3064	0.2181	0.2123	0.2661	0.4202	0.3696
	a_4	1.059	-0.0938	0.2506	-0.1504	0.2766	0.5254

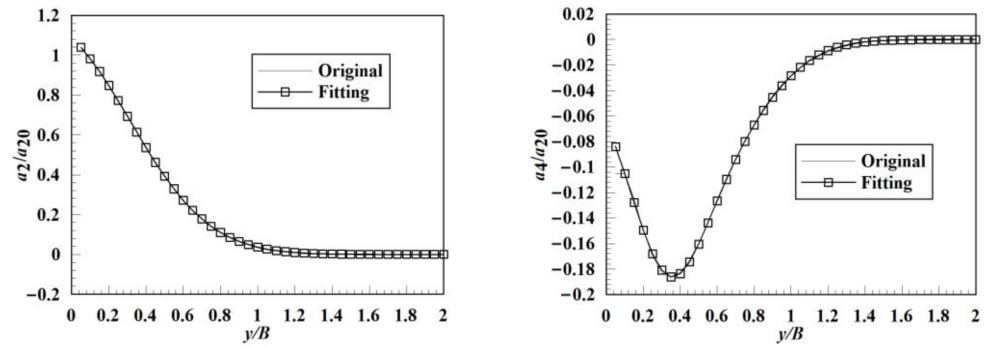


Figure 11. Fitting results of model 1.

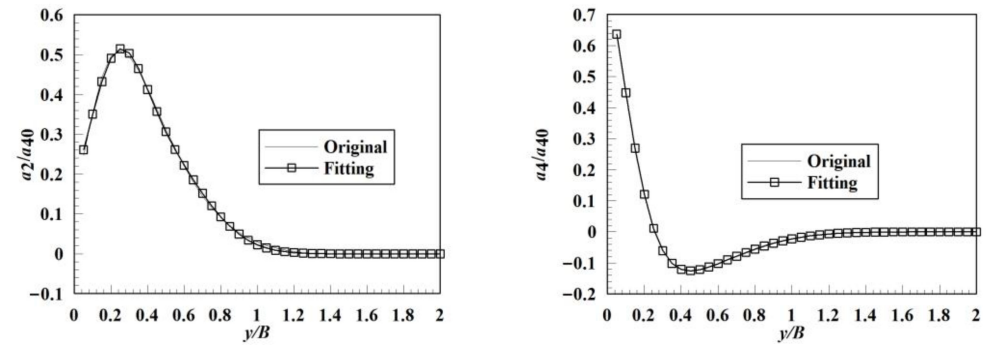


Figure 12. Fitting results of model 2.

To test the fitting precision, the case of $a_{20} = -30$ MPa, $a_{40} = 50$ MPa, $B = 1250$ mm is simulated as an example with the finite difference method and fitting equation, and the results are shown in Figure 13. It can be seen that the stress evolution regulation along the edge and at a quarter of the strip, calculated by the fitting equation, is in good agreement with that calculated by the finite difference method.

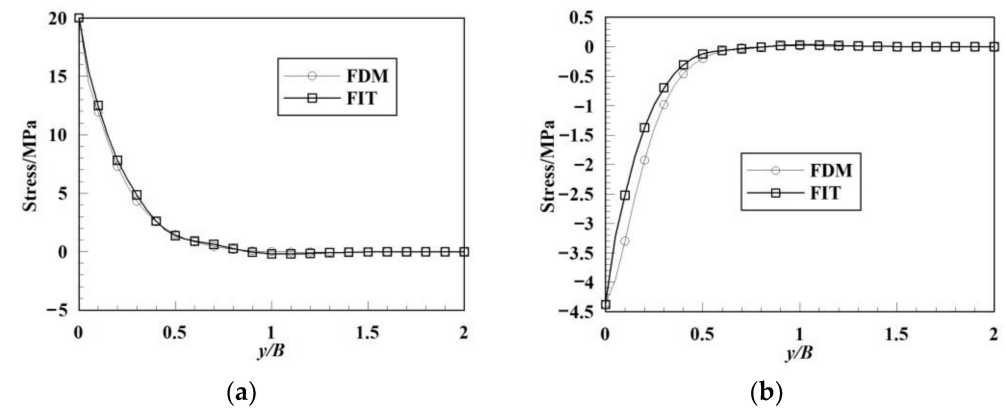


Figure 13. Comparison between finite difference method and fitting equation. (a) Edge, (b) Quarter.

To achieve accurate flatness prediction, two issues need to be studied, as shown in Figures 2 and 3. The coupling relationship between the entry and exit tensile stress distribution and the velocity in the deformation zone has been extensively studied by the authors in previous research [27]. The second issue, which is the mechanism of the flow variation of the external tensile stress and velocity distribution in the deformation zone, is the main focus of this study. According to the research results in this study, it is obvious that the tensile stress distribution in the upstream and downstream regions of the deformation zone is different from that in the entry and exit regions of the deformation zone. Specially, between the exit of the deformation zone and the downstream region, the velocity distribution gradually becomes more uniform, while the tensile stress distribution

gradually stabilizes. When the installation position of the flatness meter is sufficiently far from the exit of the deformation zone, the detection errors caused by uneven velocity can be disregarded. However, when the installation position of the flatness meter is not far enough from the exit of the deformation zone, the model proposed in this study can be utilized to eliminate flatness detection errors.

5. Experiment

5.1. Experimental Equipment and Materials

Two pieces of aluminum strips with different specifications are placed on a 265 mm two-high rolling mill. The samples' specifications are listed in Table 2, and the related equipment is shown in Figure 14. Before rolling, 15 strain gauges are adhered to the strips at certain intervals along the width direction, as shown in Figure 15. The values in this figure are the number and position of strain gauges. At the beginning of the rolling process, with the strain gauge closest to the roll gap, the strain signal is recorded with a mobile data recorder (MDR), and then the change in the tensile stress is obtained using Hooke's law.

Table 2. Sample specifications.

Sample Number	The Initial Specification			
	Length/mm	Rolling Length/mm	Width/mm	Thickness/mm
1	600	400	200	1.7
2	450	300	150	1.7

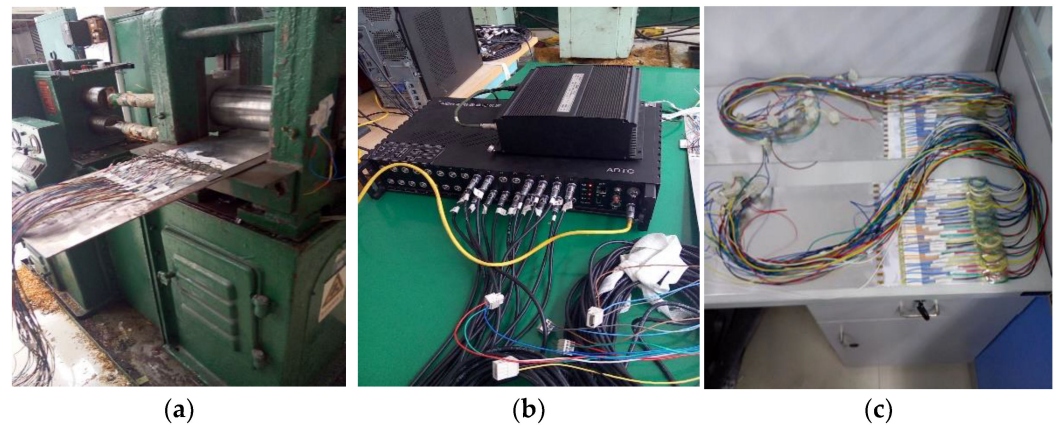


Figure 14. Equipment and materials. (a) Rolling mill. (b) MDR. (c) Aluminum strips.

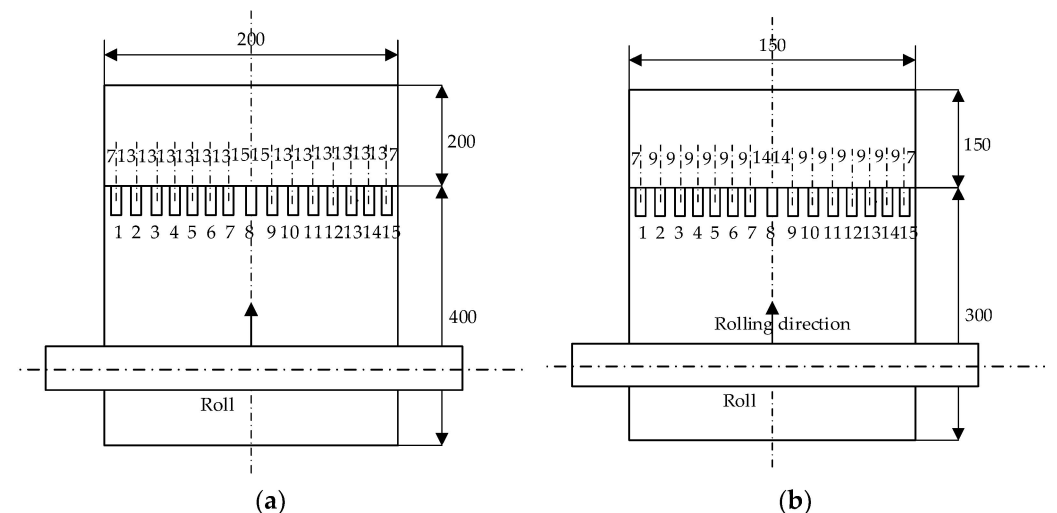


Figure 15. Distribution of strain gauges. (a) Sample 1, (b) Sample 2.

5.2. Experimental Results

For sample 1, depending on the final moment curve along the entire width of the sample, compared with that of the proposed model, which is set to $a_2 = -50.34$, $a_4 = 22.65$, the final tension stress of the experiment and model is obtained, as shown in Figure 16.

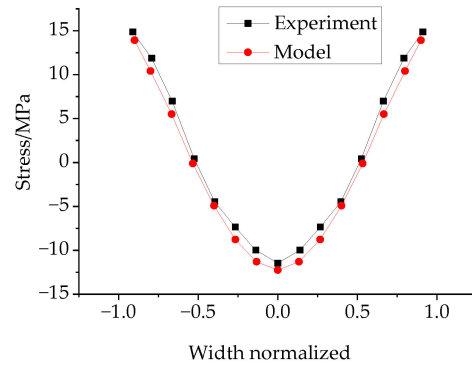


Figure 16. Final curve of entire width of sample 1.

Then, the curve of the tensile stress variation with the rolling time along the half width is established, as shown in Figure 17, where 1–8 represent the edge to the middle gauges in the half width. The two graphs in Figure 18 show the edge (strain gauge 1) and middle (strain gauge 8) stress variations.

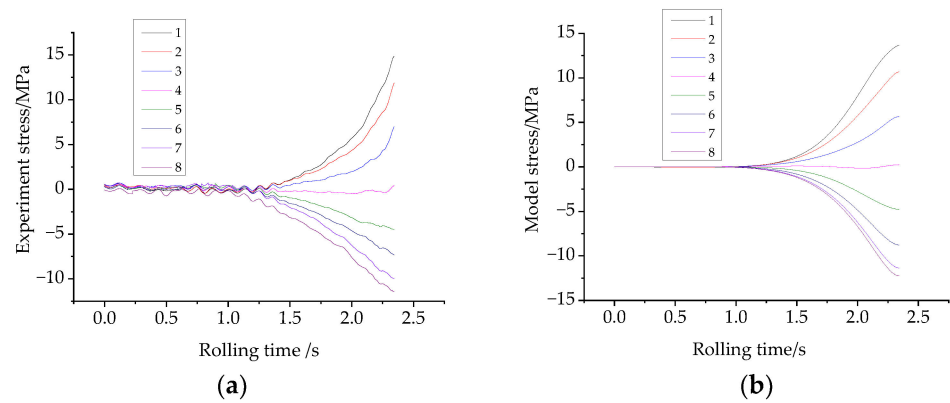


Figure 17. Stress distribution along half width of sample 1. (a) Experiment stress. (b) Model stress.

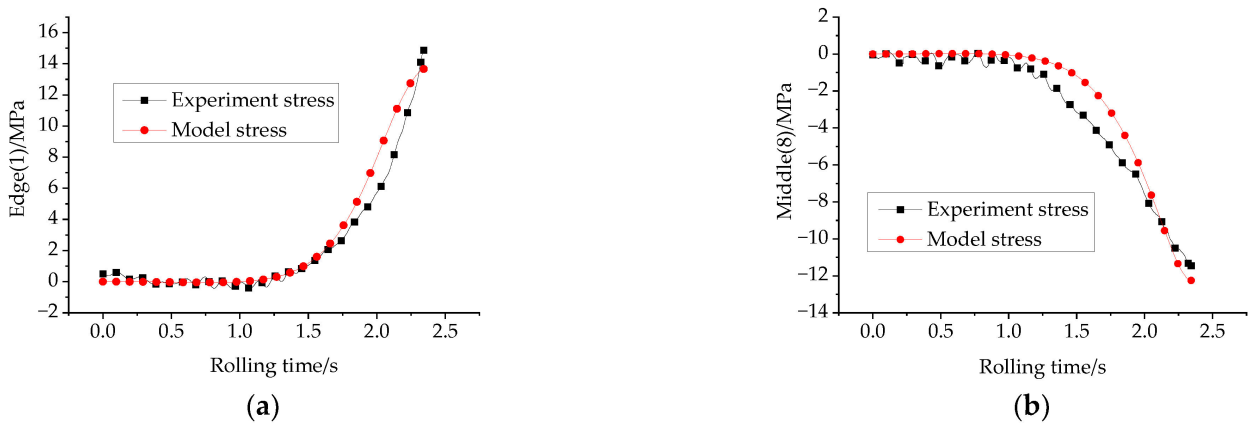


Figure 18. Comparison between model and experiment for sample 1. (a) Edge, (b) Middle.

The three-dimensional graphs of the whole process for sample 1 are presented in Figure 19.

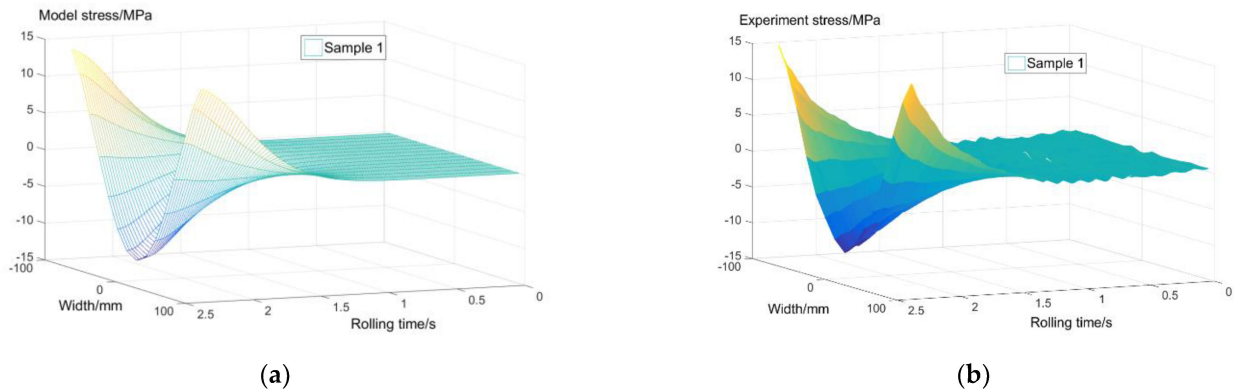


Figure 19. Stress distributions in entire process for sample 1. (a) Model, (b) Experiment.

To verify the correctness of the proposed “Gaussian” curve, the edge (strain gauge 8) is taken as an example, and the comparison between the fitting results and model results and experimental results is discussed, as shown in Figure 20. It can be seen that the simulation results calculated by the fitting equation are in good agreement with those calculated by the finite difference method and with the experimental results.

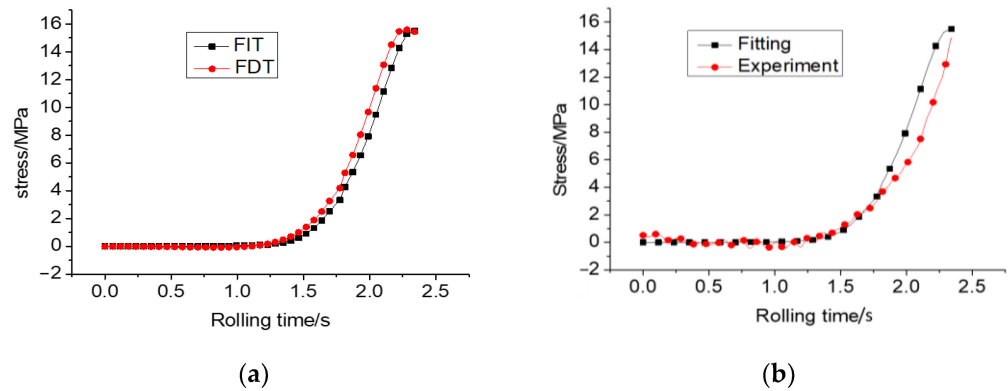


Figure 20. Comparison between fitting results and model and experimental results for sample 1. (a) Comparison with model, (b) Comparison with experiment.

With the same treatment for sample 2, which is set to $a_2 = -46.89$, $a_4 = 28.15$, the final tension stress of the experiment and model is obtained, as shown in Figure 21.

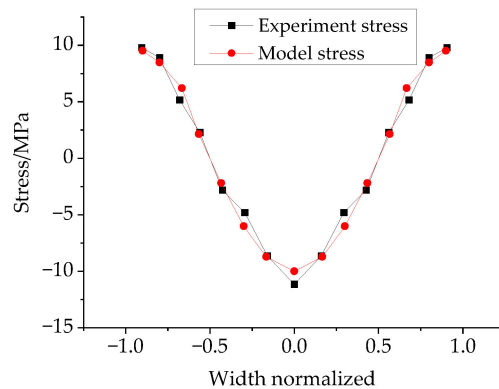


Figure 21. Final curve of whole width for sample 2.

The tensile stress variation with the rolling time along the half width is also obtained, as shown in Figure 22. The two graphs in Figure 23 show the edge (strain gauge 1) and middle (strain gauge 8) stress variations.

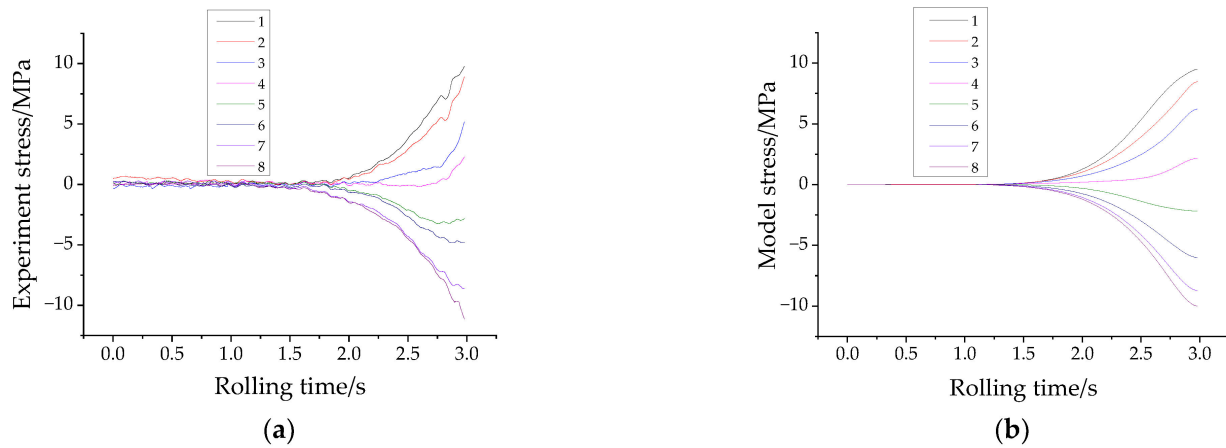


Figure 22. Stress distributions along half width for sample 2. (a) Experiment stress, (b) Model stress.

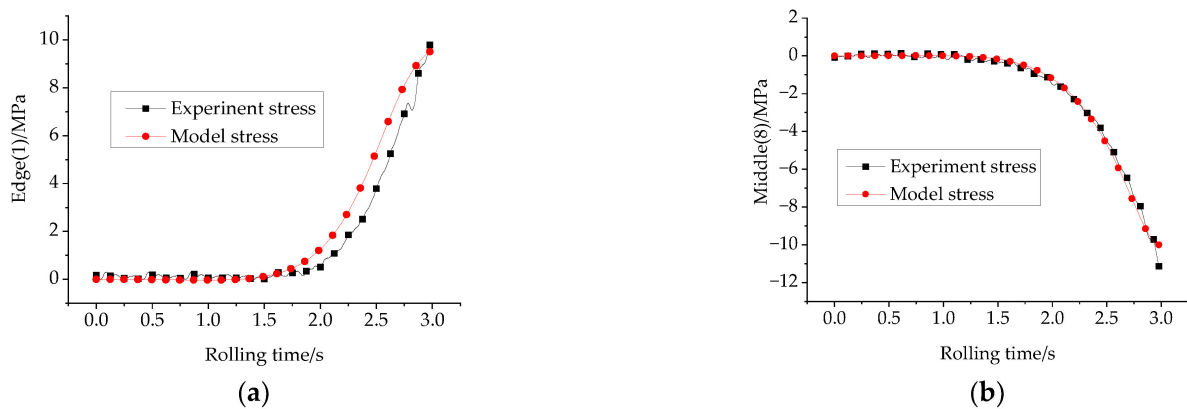


Figure 23. Comparison between model and experiment for sample 2. (a) Edge, (b) Middle.

Then, the three-dimensional graphs of the whole process for sample 2 are presented in Figure 24.

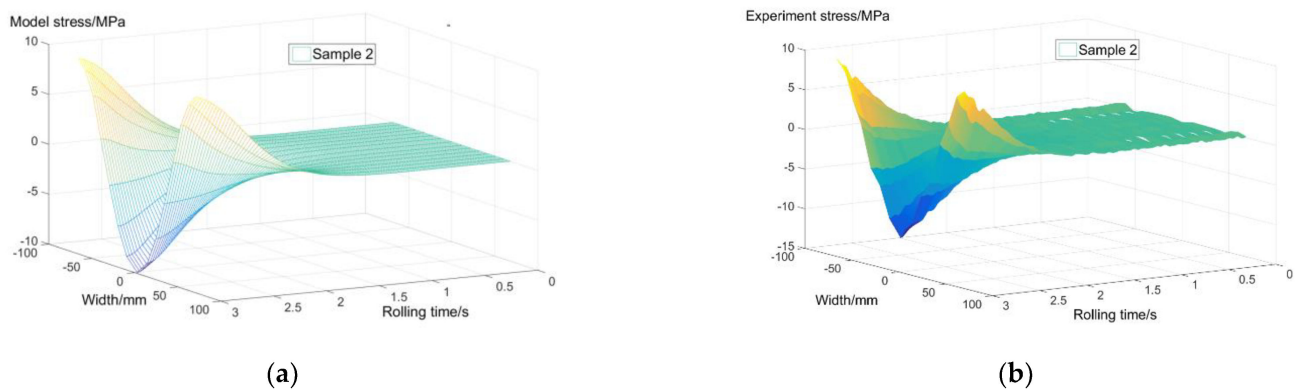


Figure 24. Stress distributions in whole process for sample 2. (a) Model, (b) Experiment.

Finally, taking the edge (strain gauge 8) as an example, the comparison between the fitting results and model results and experimental results for sample 2 is discussed in Figure 25.

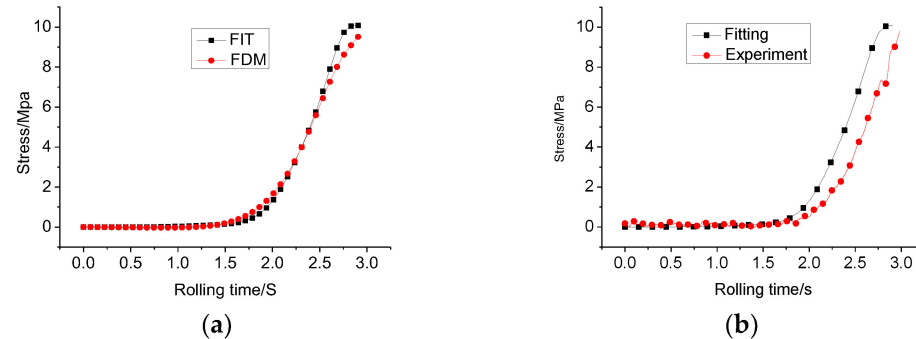


Figure 25. Comparison between fitting results and model and experimental results for sample 2. (a) Comparison with model, (b) Comparison with experiment.

5.3. Analysis

From the experimental results, it can be seen that the strain signal starts to appear at half of the rolling time, in general, because the actual roll length is twice its width; that is, the signal appears after a distance of one strip width, so it is consistent with the model. The stress variation forms of the experiment and model are nearly identical. As presented above, the experimental results fit well with the model results. The comparison of the fitting results with the model results and experimental results shows that the proposed “Gaussian” curve is accurate and practical.

6. Conclusions

1. The theoretical and experimental results show that the tensile stress distribution in the upstream and downstream regions of the deformation zone is different from that in the entry and exit regions of the deformation zone. Specially, between the exit of the deformation zone and the downstream region, the velocity distribution gradually becomes more uniform, while the tensile stress distribution gradually stabilizes.
2. The tension stress fluctuation of the strip outside the deformation zone can be regarded as a plane stress problem. A basic differential equation can be established based on the stress function method, and the finite difference method can be used to solve the differential equation. The calculated results indicate that the stress amplitude at different distances from the exit has a linear relationship with the amplitude of the initial stress, which falls roughly 98.8% after a distance of one strip width. The initial stress amplitude and strip width have little effect on the change trend of the stress evolution caused by the uneven velocity distribution, and the initial stress form is influential. The initial stress form can be broken down into two basic modes, that is, a quadratic or quartic coefficient. Any type of initial stress form can be considered as a linear combination of the two basic modes.
3. To save time, a “Gaussian” curve is proposed to fit the calculated results of the finite difference method. The simulation results reveal that the stress evolution calculated by the fitting equation is in good agreement with that calculated by the finite difference method.
4. To verify the practicability of the proposed model, a tensile stress rheology experiment is conducted, as shown above, and it can be seen that the experimental results fit well with the model results. Thus, it can be concluded that the model is correct and practical. The comparison of the fitting results with the model results and experimental results reveals that the proposed “Gaussian” curve is accurate and practical.

Author Contributions: Conceptualization, K.Z. and D.W.; methodology, K.Z. and D.W.; writing—original draft preparation, K.Z. and Y.X.; writing—review and editing, Y.X. and D.W.; supervision, D.W. and H.L.; funding acquisition, D.W. and H.L. All authors have read and agreed to the published version of the manuscript.

Funding: This work was supported by the National Natural Science foundation of China (No. U21A20118) and the National Key Laboratory of Metal Forming Technology and Heavy Equipment, China National Heavy Machinery Research Institute Co., Ltd., Xi'an (No. S2208100.W04).

Institutional Review Board Statement: Not applicable.

Informed Consent Statement: Not applicable.

Data Availability Statement: Not applicable.

Acknowledgments: Not applicable.

Conflicts of Interest: The authors declare no conflict of interest.

References

1. Sun, J.; Shan, P.F.; Wei, Z.; Hu, Y.H.; Wang, Q.L.; Peng, W.; Zhang, D.H. Data-based flatness prediction and optimization in tandem cold rolling. *J. Iron Steel Res. Int.* **2020**, *28*, 563–573. [\[CrossRef\]](#)
2. Wang, Y.S.; Xu, X.D.; Ren, B.B.; Liu, J.; Zhao, R.G. Effect of Geometrical Factors on Torsion in Cold Roll Forming of the Lower Side Beam of a Car. *Appl. Sci.* **2021**, *11*, 7852. [\[CrossRef\]](#)
3. Roh, Y.H.; Byon, S.M.; Lee, Y. Numerical Analysis of Edge Cracking in High-Silicon Steel during Cold Rolling with 3D Fracture Locus. *Appl. Sci.* **2021**, *11*, 8408. [\[CrossRef\]](#)
4. Xu, D.; Yang, Q.; Wang, X.C.; He, H.; Sun, Y.Z.; Li, W.P. An Experimental Investigation of Steel Surface Topography Transfer by Cold Rolling. *Micromachines* **2020**, *11*, 916. [\[CrossRef\]](#) [\[PubMed\]](#)
5. Wang, D.C.; Liu, H.M.; Liu, J. Research and Development Trend of Shape Control for Cold Rolling Strip. *Chin. J. Mech. Eng.* **2017**, *30*, 1248–1261. [\[CrossRef\]](#)
6. Yi, G.D.; Liang, Y.; Wang, C.; Xu, J.H. Evolution of Residual Stress Based on Curvature Coupling in Multi-Roll Levelling. *Appl. Sci.* **2019**, *9*, 4975. [\[CrossRef\]](#)
7. Shohet, K.N.; Townsend, N.A. Roll Bending Methods of Crown Control in Four-High Plate Mills. *J. Iron Steel Inst.* **1968**, *11*, 1088–1098.
8. Jiang, G.Y.; Wang, Y.Q.; Yan, X.C. Analysis on solution of residual stress for cold rolling strip. *J. Iron Steel Res.* **2010**, *22*, 16–18.
9. Xu, L.J. *Flatness Control in Cold Strip Rolling and Mill Type Selection*; Metallurgical Industry Press: Beijing, China, 2007.
10. Matsumoto, H. 2-Dimensional lateral-material-flow model reduced from 3-Dimensional theory for flat rolling. *ISIJ Int.* **1991**, *31*, 550–558. [\[CrossRef\]](#)
11. Kim, Y.K.; Kwak, W.J.; Shin, T.J.; Hwang, S.M. A new model for the prediction of roll force and tension profiles in flat rolling. *ISIJ Int.* **2010**, *50*, 1644–1652. [\[CrossRef\]](#)
12. Bryant, G.F. *Automation of Tandem Mills*; The Iron and Steel Institute: London, UK, 1973; pp. 176–212.
13. Ishikawa, T.; Tozawa, Y.; Yukawa, N.; Yamanaka, M. Analytical Approach to the Shape of Rolled Strip. In *Advanced Technology of Plasticity*; Springer: Berlin/Heidelberg, Germany, 1984; pp. 1161–1166.
14. Liu, X.H.; Jiang, Z.Y.; Wang, G.D. Analysis of 3-D Deformation for Crowning Strip Rolling by Rigid-Plastic FEM. In *Advanced Technology of Plasticity*; Springer: Berlin/Heidelberg, Germany, 1993; pp. 717–720.
15. Wang, D.C.; Liu, H.M. A model coupling method for shape prediction. *J. Iron Steel Res. Int.* **2012**, *19*, 22–27. [\[CrossRef\]](#)
16. Lian, J.C. Analysis of profile and shape control in flat rolling. In Proceedings of the First International Conference on Steel Rolling, Tokyo, Japan, 29 September–4 October 1980; The Iron and Steel Institute of Japan: Tokyo, Japan, 1980; Volume 2, pp. 713–720.
17. Liu, H.M.; Chen, S.W.; Peng, Y.; Sun, J.L. Strip layer method for analysis of the three-dimensional stresses and spread of large cylindrical shell rolling. *Chin. J. Mech. Eng.* **2015**, *28*, 556–564. [\[CrossRef\]](#)
18. Liu, H.M.; Lian, J.C.; Duan, Z.Y. Study on the transverse distributions of front and back tensions in strip rolled 4-high mill. *Heavy Mach.* **1989**, *4*, 12–20.
19. Liu, H.M. *Three Dimensional Rolling Theory and Application*; Science Press: Beijing, China, 1999; pp. 1–53, 276–283.
20. Ishikawa, T.; Nakamura, M.; Tozawa, Y. Three-dimensional analysis of sheet rolling considering roll deformation. *Plast. Process.* **1980**, *21*, 902–908.
21. Cresdee, R.B.; Wdwards, W.J.; Thomas, P.J. An advanced model for flatness and profile prediction in hot rolling. *Iron Steel Eng.* **1991**, *68*, 41–45.
22. Yuen, W.Y.; Cozijnsen, M. Strip Shape Analysis in Cold Rolling. In Proceedings of the 44th Mechanical Working and Steel Processing Conference Proceedings, Orlando, FL, USA, 8–11 September 2002.
23. Tarnoplskaya, T.F.; Hoog, R.D. An efficient method for strip flatness analysis in cold rolling. *Math. Eng. Ind.* **1998**, *7*, 71–95.
24. Cao, H.D. *Plastic Deformation Mechanics Basis and Rolling Theory*; Mechanical Industry Press: Beijing, China, 1981; pp. 151–159.

25. Domanti, S.; Mcelwain, D.S.; Middleton, R.H.; Edwards, W.J. The decay of stresses induced by flat rolling of metal strip. *Int. J. Mech. Sci.* **1993**, *35*, 897–907. [[CrossRef](#)]
26. Li, W.T.; Huang, B.H.; Bi, Z.B. *Analysis and Application of Thermal Stress Theory*; China Electric Power Press: Beijing, China, 2006; pp. 115–128.
27. Wang, D.C. Entry and exit stress variation of cold rolling strip. *J. Iron Steel Res. Int.* **2012**, *19*, 19–24. [[CrossRef](#)]

Disclaimer/Publisher’s Note: The statements, opinions and data contained in all publications are solely those of the individual author(s) and contributor(s) and not of MDPI and/or the editor(s). MDPI and/or the editor(s) disclaim responsibility for any injury to people or property resulting from any ideas, methods, instructions or products referred to in the content.